SCIENCE CHINA Materials ARTICLES

mater.scichina.com link.springer.com

Published online 22 October 2019 | https://doi.org/10.1007/s40843-019-1178-5
Sci China Mater 2020, 63(2): 267–275

Structure-induced hollow Co_3O_4 nanoparticles with rich oxygen vacancies for efficient CO oxidation

Zhijie Chen, Yajing Wang, Qiannan Liang, Liyu Chen, Weiteng Zhan and Yingwei Li*

ABSTRACT **Co_3O_4 has been considered as one kind of promising catalysts for the oxidation of CO. According to the Mars-van Krevelen mechanism, oxygen vacancies of Co_3O_4 play a significant role in catalytic activity. Herein, we report a novel structure-induced strategy to develop hollow Co_3O_4 with rich oxygen vacancies for efficient oxidation of CO. Through a reduction-oxidation pyrolysis process, the metal-organic frameworks (MOFs) precursor (i.e., ZIF-67) is transformed into H-Co_3O_4@H-C, in which hollow Co_3O_4 (H-Co_3O_4) nanoparticles (NPs) are embedded in hollow carbon (H-C) shell. The hollow Co_3O_4 NPs feature rich oxygen vacancies and finish a complete conversion of CO at 130°C, which is much lower than that of solid Co_3O_4 (the temperature of full CO conversion T_{100}=220°C). Besides, the hollow carbon shell could also reduce the diffusion resistance during the oxidation process. Benefiting from the unique hollow structures, H-Co_3O_4@H-C even shows comparable activity to noble metal catalysts under high weight hourly space velocities (WHSVs) up to 240,000 mL h^{-1} $g_{cat.}^{-1}$. Furthermore, the H-Co_3O_4@H-C catalyst also shows good durability with only a slight decline after the reaction has been operated for 24 h.**

Keywords: CO oxidation, metal-organic frameworks, cobalt oxide, hollow structure, oxygen vacancy

INTRODUCTION

With the development of modern industry, oxidation of carbon monoxide is increasingly important in relation to in-door air quality control and automotive emissions purification. Tricobalt tetraoxide (Co_3O_4) has been demonstrated to be an efficient catalyst for the oxidation of CO [1–4]. It is generally accepted that the CO oxidation catalyzed by Co_3O_4 proceeds *via* the Mars-van Krevelen mechanism, in which the oxygen vacancies on the surface of Co_3O_4 can activate O_2 molecules to form actively adsorbed oxygen (O_{ads}) that would react with CO adsorbed on Co^{3+} ions to produce CO_2 [5–7]. The initial oxygen vacancies determine the amount of O_{ads} on the surface of Co_3O_4 to affect the activity of CO oxidation [8–10]. In this regard, it is desirable to effectively enrich the oxygen vacancies on the surface of Co_3O_4.

The traditional way to create oxygen vacancies on the surface of Co_3O_4 is to calcine Co_3O_4 at high temperature [11]. During the calcination process, some oxygen species on the Co_3O_4 surface would release to form oxygen vacancies. However, the treatments at high temperatures would inevitably result in severe agglomeration of Co_3O_4. Besides, it has been reported that the surface atomic configuration of Co_3O_4 was strongly influenced by its morphology [12]. Specially, metal oxides with hollow structures were demonstrated to possess more defect sites on their surfaces than the solid counterparts [13–18]. Therefore, we could reasonably speculate that fabrication of Co_3O_4 with hollow structure may maximize the oxygen vacancies on its surface to achieve high catalytic efficiency in CO oxidation.

Recently, metal-organic frameworks (MOFs), constructed by inorganic nodes with organic linkers, have been used as versatile templates for preparing a variety of functional materials, including metal oxides [19–27]. Through controlling the pyrolysis atmosphere and temperatures, metal oxides with different morphologies could be synthesized [28–31], providing great opportunity to tune their exposed surface configurations with enriched oxygen vacancies. In this work, we report a novel structure-induced strategy to enrich the surface oxygen vacancies through fabricating Co_3O_4 NPs with hollow structure derived from MOFs. As a proof of concept, we selected a Co-based MOF (i.e., ZIF-67) as the precursor for the synthesis of hollow Co_3O_4 NPs embedded in hollow carbon shell (denoted as H-Co_3O_4@H-C) *via* a reduction-oxidation pyrolysis process. The hollow Co_3O_4 structure possessed rich oxygen vacancies on the surface

State Key Laboratory of Pulp and Paper Engineering, School of Chemistry and Chemical Engineering, South China University of Technology, Guangzhou 510640, China
* Corresponding author (email: liyw@scut.edu.cn)

 © Science China Press and Springer-Verlag GmbH Germany, part of Springer Nature 2019

for the activation of O_2, and the hollow carbon shell enhanced the substrate diffusion and also stabilized the hollow Co_3O_4 NPs during the oxidation process. The resulting H-Co_3O_4@H-C composites showed excellent catalytic activity and durability for CO oxidation, achieving a complete CO conversion at 130°C and a high weight hourly space velocity (WHSV) of 60,000 mL h^{-1} $g_{cat.}^{-1}$ for up to 24 h of reaction time, representing a highly efficient catalyst for CO oxidation.

EXPERIMENTAL SECTION

All chemicals used in this work were purchased from commercial sources (Sigma-Aldrich, Alfa Aesar, and others) and used without further purification.

Materials synthesis

In a typical synthesis of ZIF-67, cobalt nitrate hexahydrate (875.4 mg, 3 mmol) and 2-methylimidazole (990 mg, 12 mmol) were dissolved into 75 mL of methanol, respectively. Then the two solutions were quickly mixed. After being stirred for a few seconds, the mixed solution was left for aging for 24 h at room temperature. The resulting purple precipitates were collected by centrifugation, subsequently washed with methanol for 3 times, and finally dried under vacuum at 80°C for 24 h.

H-Co_3O_4@H-C was synthesized by using a reduction-oxidation method. 0.5 g of ZIF-67 was placed in a tubular furnace and then heated at 600°C for 3 h with a heating rate of 2°C min^{-1} under an Ar/H_2 (90%/10% in volume ratio) atmosphere. After the temperature was cooled to 350°C, the Ar/H_2 atmosphere was changed to air and held for 10 min. Then an argon atmosphere was introduced instead of air to end up the oxidation process and the heating program was stopped.

For comparison purpose, another two samples were prepared by using ZIF-67 as precursors. The synthesis of H-Co_3O_4@C was the same as that of H-Co_3O_4@H-C except that the Ar/H_2 was replaced by pure Ar at the beginning. Co_3O_4@H-C was prepared according to the previous report with minor modifications [32]. 0.5 g of ZIF-67 was placed in a tubular furnace and then heated at 450°C for 2 h with a heating rate of 2°C min^{-1} under air. After being cooled down to room temperature, the Co_3O_4@H-C material was obtained.

Co@C-Ar/H_2 or Co@C-Ar was obtained directly by calcinating ZIF-67 under an Ar/H_2 or Ar atmosphere at 600°C for 3 h, respectively.

Materials characterization

Powder X-ray diffraction (XRD) patterns of the samples were recorded with a Rigaku (40 kV, 30 mA, 0.1534 nm) using Cu Kα radiation. The Brunauer-Emmett-Teller (BET) surface area and pore size distribution were measured using N_2 adsorption/desorption isotherms at −196.15°C on a Micromeritics ASAP 2020M instrument. Before the mensuration, the samples were degassed at 150°C for 4 h. X-ray photoelectron spectroscopy (XPS) with a Thermo ESCALAB 250XI multifunctional imaging electron spectrometer was used to analyze the electronic states and the surface interaction among the elements of the samples. The binding energies of all elements were calibrated with the C 1s peak at 284.8 eV. The Co contents of the samples were determined quantitatively by atomic absorption spectroscopy (AAS) on a HITACHI Z-2300 instrument. Temperature-programmed reduction by H_2 (H_2-TPR) was performed on a DAS-7200 from HUASI Instruments. Typically, 5.0 mg of sample was pretreated in a flow of N_2 at 200°C for 0.5 h with a heating rate of 5°C min^{-1} to remove adsorbed water and other impurities. After being cooled down to room temperature, the sample was heated from room temperature with a ramp rate of 10°C min^{-1} to 800°C under a flow of Ar/H_2 (90%/10% in volume ratio). Transmission electron microscopy (TEM) images were taken on a JEOL 2100F analytical electron microscope operated at 200 kV. A high-resolution scanning electron microscope (SEM, Hatachi SU8220) was used to observe the morphology of the samples.

Catalytic tests

The catalytic activities of the samples for CO oxidation were measured in a fixed bed micro-reactor (9 mm i.d.) under ambient pressure. Typically, 50 mg of the catalyst was loaded into the reactor and pretreated in N_2 at 200°C for 2 h to remove moisture and adsorbed impurities. After being cooled to room temperature, a gas mixture containing 1 vol% CO and 99 vol% air were introduced into the reactors at a flow rate of 50 mL min^{-1} using mass flow controllers, corresponding to a WHSV of 60,000 mL $g_{cat.}^{-1}$ h^{-1}. The composition of the effluent gases was monitored using an online gas chromatograph equipped with a thermal conductivity detector (TCD). The catalytic data were collected after 30 min for each temperature to ensure a steady-state condition. For the stability test, the reactions were conducted under the same reaction conditions as described above.

RESULTS AND DISCUSSION

Scheme 1 illustrated the synthetic routes for preparing cobalt-based materials using ZIF-67 as template. Among

 © Science China Press and Springer-Verlag GmbH Germany, part of Springer Nature 2019

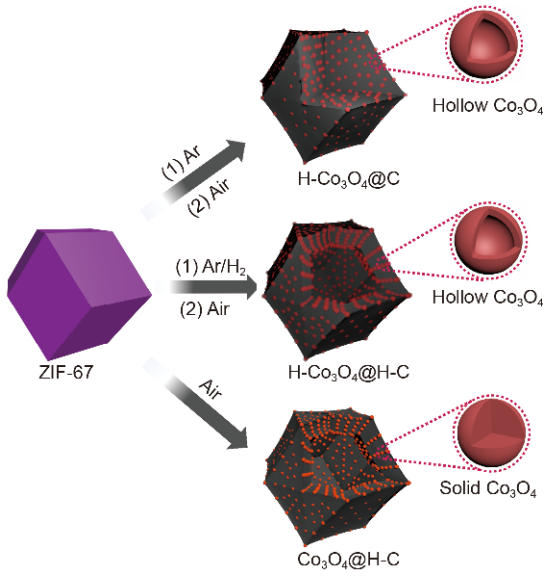

Scheme 1 Synthetic routes of H-Co_3O_4@C, H-Co_3O_4@H-C, and Co_3O_4@H-C.

these MOF-derived materials, H-Co_3O_4@H-C was prepared through a reduction-oxidation pyrolysis process. ZIF-67 was first treated in Ar/H_2 at 600°C. During this step, the cobalt cations in the ZIF-67 frameworks were reduced into Co NPs, as was evident from the XRD pattern of Co@C-Ar/H_2 (Fig. S1). Then, air was introduced as oxidant to implement the succedent oxidation at 350°C to yield H-Co_3O_4@H-C. From the XRD pattern of H-Co_3O_4@H-C in Fig. 1a, it was clear to identify that the Co NPs were transformed into Co_3O_4 NPs within a short time of oxidation.

For comparisons, another two cobalt-based catalysts (H-Co_3O_4@C and Co_3O_4@H-C) were prepared by using different calcination processes. For the synthesis of H-Co_3O_4@C, a similar preparation method as for H-Co_3O_4@H-C was employed, only altering the initial atmosphere for Ar/H_2 to Ar (Scheme 1). Thus Co@C-Ar was obtained after the pyrolysis of ZIF-67 under Ar atmosphere and then the followed oxidation converted the Co NPs into Co_3O_4 NPs inside the final H-Co_3O_4@C catalyst (Fig. S1 and Fig. 1a). It is worth noting that the average sizes of Co NPs inside Co@C-Ar/H_2 and Co@C-Ar increased after oxidation as compared with those of Co_3O_4 NPs in H-Co_3O_4@H-C and H-Co_3O_4@C (Table 1), respectively. These results indicated that re-construction might happen to the inner structure of those NPs during the transformation. The Co_3O_4@H-C was synthesized

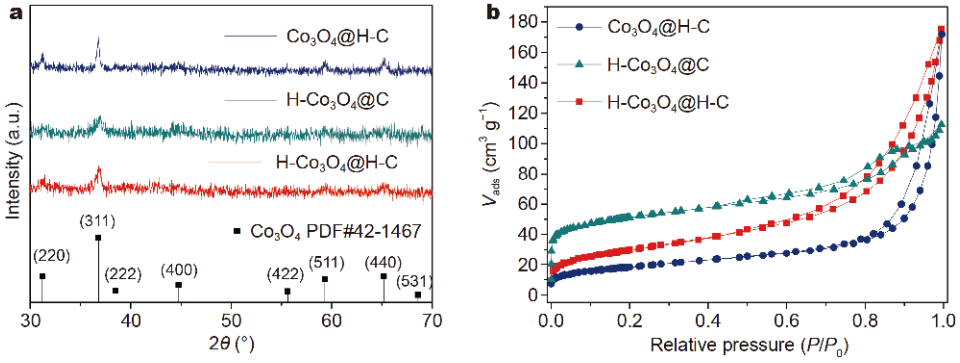

Figure 1 (a) XRD patterns of Co_3O_4@H-C, H-Co_3O_4@C, and H-Co_3O_4@H-C; (b) N_2 adsorption/desorption isotherms of Co_3O_4@H-C, H-Co_3O_4@C, and H-Co_3O_4@H-C.

Table 1 Physicochemical properties and CO oxidation activities of the Co-based catalysts

Samples	BET surface area (m^2 g^{-1})	Crystalline domain size[a] (nm)	Co content[b] (wt%)	O_{ads}/O_{latt} molar ratio[c]	T_{100}[d] (°C)
Co@C600-Ar/H_2	192	15.1	44.2	–	–
H-Co_3O_4@H-C	104	19.0	50.3	1.15	130
H-Co_3O_4@ C	172	18.9	46.8	0.98	170
Co_3O_4@H-C	51	23.5	60.0	0.44	220

a) Cobalt crystalline size was calculated from XRD reflection broadening with the Scherrer equation; b) Co contents were measured by AAS; c) O_{ads}/O_{latt} (lattice oxygen) molar ratio was calculated based on the XPS results; d) reaction condition: 1 vol% CO balanced by air, $m_{cat.}$=50 mg, WHSV=60,000 mL h^{-1} $g_{cat.}^{-1}$.

 © Science China Press and Springer-Verlag GmbH Germany, part of Springer Nature 2019

directly under air atmosphere at 450°C and the cobalt compounds were assigned to Co_3O_4 (Fig. 1a).

Although different calcination processes were applied, H-Co_3O_4@H-C, H-Co_3O_4@C and Co_3O_4@H-C displayed similar porous structures. As shown in Fig. 1b, these cobalt-based materials all displayed low adsorption capacities at low relative pressures, which indicated that the catalysts possessed micropores in their structures. At high relative pressures, all three catalysts exhibited hysteresis loops that could be associated with the existence of mesopores, as evident from the pore distribution curves (Fig. S2) [33–35]. The BET surface areas of the cobalt-based materials are listed in Table 1. Interestingly, the Co content followed the order of H-Co_3O_4@C < H-Co_3O_4@H-C < Co_3O_4@H-C, which was opposite to that of their BET surface areas. It probably reflected that H-Co_3O_4@C could preserve the porous structure from the template to a greater extent with more loss of the carbon and nitrogen elements resulting in a higher Co content.

In order to investigate the morphology evolution, SEM and TEM were employed to observe the formation of the hollow cavities. After pyrolysis under Ar/H_2, the obtained Co@C-Ar/H_2 (Fig. S3d–f) still preserved the rhomboic dodecahedron morphology of the template ZIF-67 (Fig. S3a–c), while generating a hollow cavity with a size of ca. 300 nm. It was proposed that, in presence of H_2, the Co species in ZIF-67 was reduced at relative low temperatures and accelerated the pyrolysis process of imidazole ligands and the consumption of carbon [36]. With subsequent introduction of air instead of the reduction gas, the hollow skeleton of Co@C-Ar/H_2 was maintained (Fig. 2a, d). Meanwhile, hollow Co_3O_4 NPs were formed inside the H-Co_3O_4@H-C material (Fig. 2g). TEM and high-resolution TEM (HRTEM) images of the Co_3O_4 NPs in H-Co_3O_4@H-C (Fig. 3) were taken to observe their structures. It was clear to note that most of the Co_3O_4 NPs in Fig. 3a possessed a hollow cavity inside the Co_3O_4 shell, which should be the reason that the average sizes of NPs increased after the oxidation (Table 1). The HRTEM image in Fig. 3b showed a lattice spacing of 0.233 nm, which could be attributed to the (222) plane of Co_3O_4.

Solid carbon shells were obtained in H-Co_3O_4@C (Fig. 2b, e, h) when the calcination atmosphere was changed to pure Ar, demonstrating that the presence of H_2 was crucial to fabricate hollow carbon shells. However, hollow Co_3O_4 NPs were observed in both H-Co_3O_4@H-C and H-Co_3O_4@C, which proved that short time of the oxidation process played a significant role. According to the previous reports [37–40], the formation of small cavities in Co_3O_4 particles was caused by the different

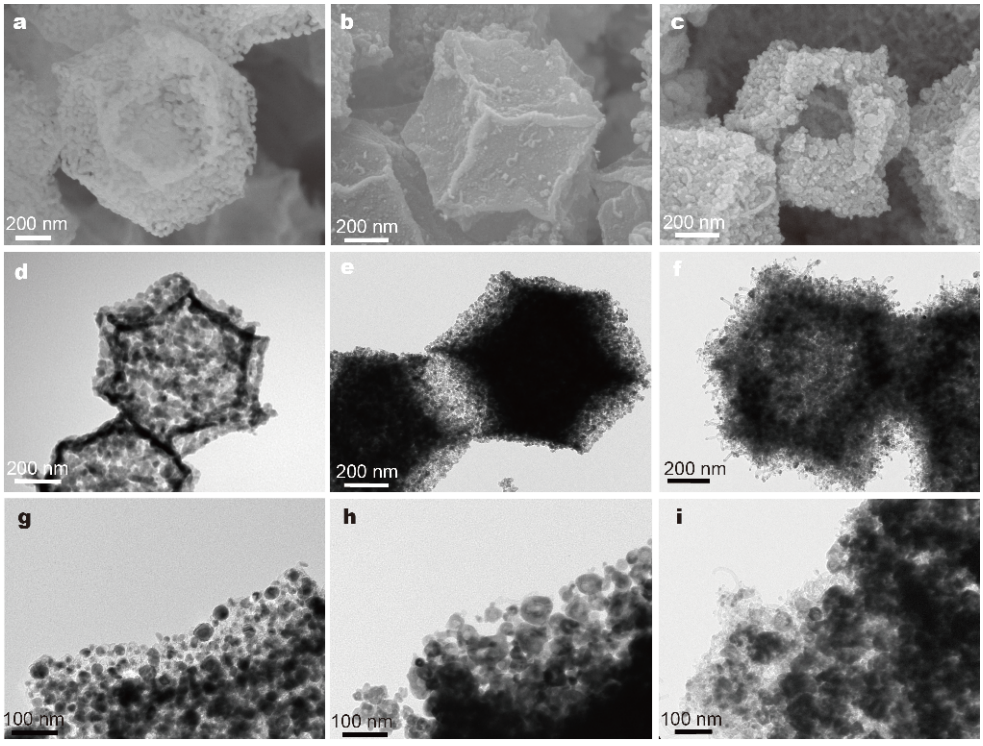

Figure 2 SEM (a–c) and TEM (d–i) images of Co_3O_4@H-C (a, d, g), H-Co_3O_4@C (b, e, h), and H-Co_3O_4@H-C (c, f, i).

© Science China Press and Springer-Verlag GmbH Germany, part of Springer Nature 2019

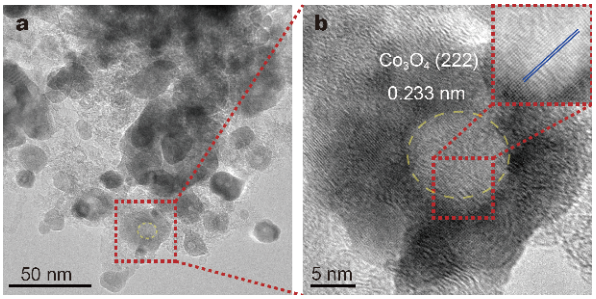

Figure 3 TEM (a) and HRTEM (b) images of H-Co_3O_4@H-C.

diffusion rates during the oxidation of Co NPs. The faster migratory rate of Co atoms to the surface as compared with that of O atoms to the core is well-known as the Kirkendall effect. Direct calcination under air atmosphere could only yield a hollow carbon shell with solid Co_3O_4 NPs, e.g., Co_3O_4@H-C, as shown in Fig. 2c, f, i. The formation mechanism of hollow carbon shell in Co_3O_4@H-C, which was different from that of H-Co_3O_4@H-C, resulting from non-equilibrium heat treatment in which two forces with the opposite direction that led to the interface separation of the Co_3O_4 shell formed at the initial stage and the ZIF-67 core [28]. The high-angle annular dark field (HAADF)-STEM images (Fig. 4) showed that both H-Co_3O_4@H-C and Co_3O_4@H-C possessed a hollow carbon shell. Energy dispersive spectrometer (EDS) mapping images of these three catalysts demonstrated that the elements of C, Co, N, and O were all evenly distributed on their bulk particles.

After structural characterizations, the catalytic performances of the as-synthesized H-Co_3O_4@H-C, Co_3O_4@H-C, and H-Co_3O_4@C materials in CO oxidation were then investigated to disclose the relationship between their structures and catalytic activities. The reactions were carried out under 1 vol% CO and 99 vol% dry air with a space velocity of 60,000 mL h^{-1} $g_{cat.}^{-1}$. As shown in Fig. 5, using H-Co_3O_4@H-C as the catalyst, the oxidation process of CO began at 50°C and completed at 130°C (the temperature of full CO conversion, T_{100}). For Co_3O_4@H-C, 100% conversion of CO was accomplished at 220°C. The apparently higher catalytic activity achieved on H-Co_3O_4@H-C suggested that the hollow cavities in Co_3O_4 NPs played a significant role in enhancing the activity. Although H-Co_3O_4@C also possessed hollow Co_3O_4 NPs, the lack of hollow cavity of carbon shell would affect the inner diffusion of the gases, resulting in lower activity (T_{100}=170°C) as compared with H-Co_3O_4@H-C.

The surface chemical states of Co and O elements can provide important information for the activity of the catalysts for CO oxidation. In general, it is believed that Co^{3+} is essential to the adsorption of CO molecule so that the oxidation could happen with the oxygen atom next to Co^{3+} [41]. For the oxygen element, three kinds of oxygen, i.e., O_{latt}, O_{ads}, and physisorbed and chemisorbed water

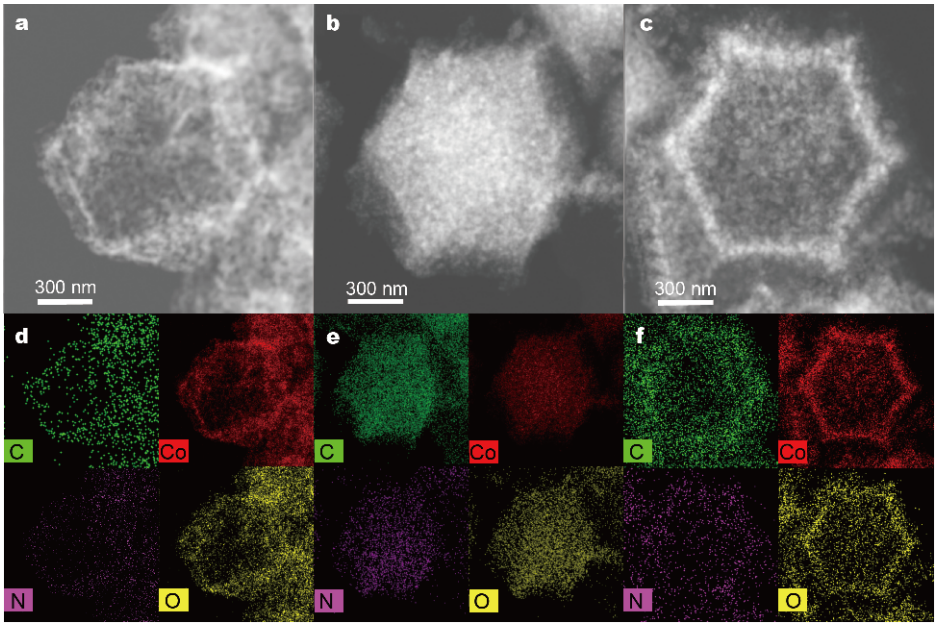

Figure 4 HAADF-STEM (a–c) and EDS (d–f) mapping images of Co_3O_4@H-C (a, d), H-Co_3O_4@C (b, e), and H-Co_3O_4@H-C (c, f).

 © Science China Press and Springer-Verlag GmbH Germany, part of Springer Nature 2019

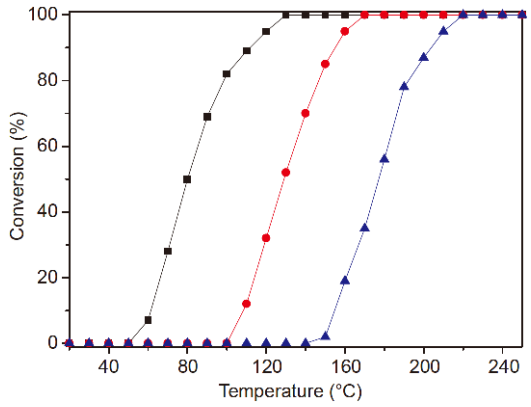

Figure 5 CO conversion as a function of reaction temperature for Co_3O_4@H-C (▲), H-Co_3O_4@C (●), and H-Co_3O_4@H-C (■). Reaction condition: 1 vol% CO balanced by air, $m_{cat.}$=50 mg, and WHSV= 60,000 mL h^{-1} $g_{cat.}^{-1}$.

(O_{wat}), may exist in the Co_3O_4. Among them, the content of O_{ads} could reflect the amount of the initial oxygen vacancies on the catalyst surfaces. Besides, the O_{ads} is considered to own higher mobility than the O_{latt} so that it could react with CO adsorbed on Co^{3+} to generate oxygen vacancies more quickly [42]. Therefore, the balance between the contents of Co^{3+} and O_{ads} is essential for the high activity of CO oxidation, as the equilibrium between CO capture and oxygen supplement could reach the highest efficiency.

To figure out the impact of Co^{3+} and initial oxygen vacancies, XPS analysis was used to determine the surface chemical states of the cobalt-based catalysts. As shown in Fig. 6a, the compositions of H-Co_3O_4@H-C, Hb-Co_3O_4 @C, and H-Co_3O_4@C were identical with C, N, O and Co as the main elements whose binding energies were 284.48, 399.44, 540.67, and 780.24 eV, respectively. According to the literature [11], the Co $2p_{3/2}$ peak could be fitted with five peaks that were at 779.85, 780.90, 782.40, 786.85 and 790.10 eV, assigning to Co^{3+}, both of Co^{3+} and Co^{2+}, Co^{2+}, satellite peak 1 (Sat. 1), and satellite peak 2 (Sat. 2), respectively (Fig. 6b). The values of the relative areas of these five peaks are listed in Table S1. Co_3O_4@H-C calcined directly under dry air possessed higher Co^{3+} content compared with H-Co_3O_4@H-C and H-Co_3O_4@C. Taking the catalytic behaviors into consideration, the content of Co^{3+} in these catalysts seemed to be enough to capture CO from the reaction gas, while the oxygen supplement was limited. Therefore, the content of the O_{ads} was regarded as the key to affect the catalytic activity

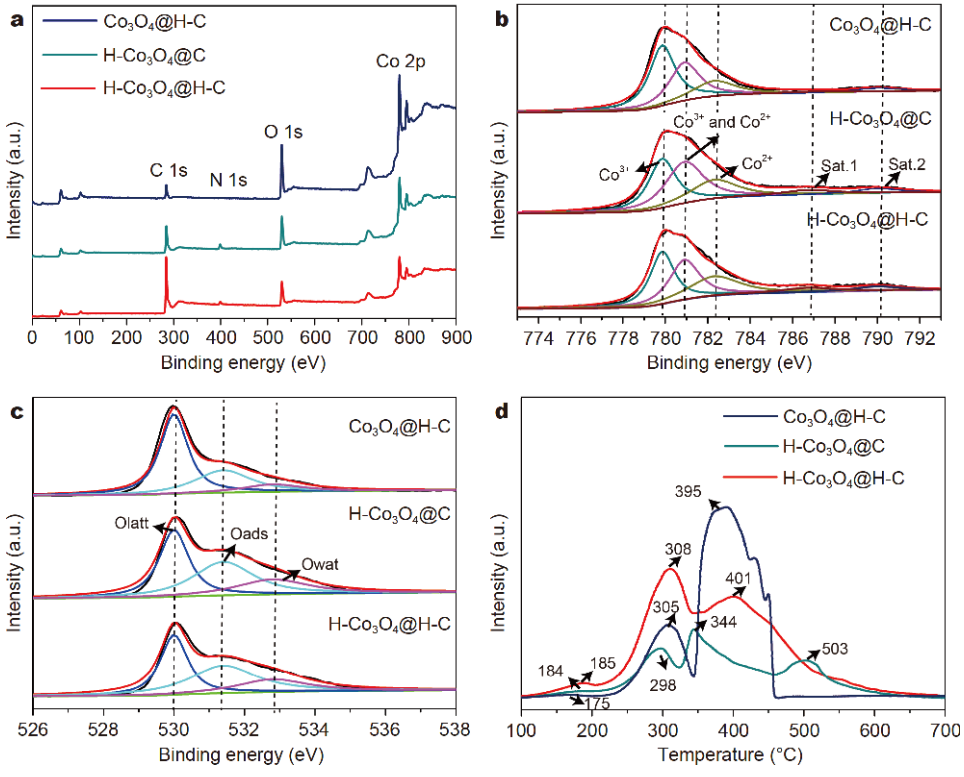

Figure 6 (a) XPS full spectrum analysis; XPS spectra of (b) Co $2p_{2/3}$, (c) O 1s; (d) H_2-TPR profiles for Co_3O_4@H-C, H-Co_3O_4@C, and H-Co_3O_4@H-C.

© Science China Press and Springer-Verlag GmbH Germany, part of Springer Nature 2019

of CO oxidation.

In Fig. 6c, the XPS spectra of O 1s were fitted with three types of peaks, including the O_{latt} at 530.00 eV, O_{ads} at 531.40 eV, and O_{wat} at 532.80 eV. The O_{ads}/O_{latt} molar ratios (Table 1) were calculated from their relative area to evaluate the quantity of initial oxygen vacancies on the catalyst surface [10]. As excepted, H-Co_3O_4@H-C owned the highest value of the O_{ads}/O_{latt} molar ratio among these three catalysts, which was 2.6 times higher than that of Co_3O_4@H-C. It has been reported that more Co^{2+} on Co_3O_4 surface would result in more oxygen vacancies [8]. Combined with the Co $2p_{2/3}$ XPS analysis, Co_3O_4@H-C showed more Co^{3+} but fewer Co^{2+} which caused fewer oxygen vacancies on its surface. The H-Co_3O_4@H-C catalyst with hollow Co_3O_4 NPs showed higher O_{ads}/O_{latt} molar ratio than Co_3O_4@H-C, which demonstrated that the structure-induced strategy could successfully affect the quantity of initial oxygen vacancies by introducing the hollow structure into Co_3O_4 NPs.

Apart from XPS analysis, H_2-TPR was employed to study the oxygen species in the cobalt-based materials. Normally, the profile of Co_3O_4 consisted of three peaks which were assigned to the reductions of adsorbed oxygen, Co_3O_4 to CoO, and CoO to Co, respectively [11,43]. The peaks below 200°C in Fig. 6d could be recognized as the reaction of the adsorbed oxygen with H_2. Their peak areas were supposed to correspond roughly to the quantity of O_{ads}. As shown in Fig. 6d, the order of peak intensities was H-Co_3O_4@H-C > H-Co_3O_4@C > Co_3O_4@H-C, which was consistent with the XPS results (Table S1). Interestingly, it was found that although H-Co_3O_4@C possessed similar hollow Co_3O_4 NPs as H-Co_3O_4@H-C, it had fewer O_{ads} than the latter. H-Co_3O_4@C could be affected by the structure of carbon materials that might cover some oxygen vacancies for adsorbing oxygen species. These results indicated that H-Co_3O_4@H-C possessed the most oxygen vacancies initially, producing more O_{ads} to activate the CO oxidation cycle.

In view of the significant effect of WHSV on catalytic behaviors, the H-Co_3O_4@H-C catalyst was tested in CO oxidation at different WHSVs. The values of T_{100} for each reaction were recorded and displayed in Fig. 7a. Generally, the catalytic activity was lowered when the WHSV increased because of the shortened residence time of reaction gas on the surface of the catalyst. For the H-Co_3O_4@H-C catalyst, the T_{100} value was enhanced from 130 to 200°C when the WHSV increased from 60,000 to 240,000 mL h^{-1} $g_{cat.}^{-1}$. Up to now, there are few reports achieving high activity for CO oxidation at relatively high WHSVs [44,45]. For example, Yan *et al.* [42] prepared a Pt/CeO_2 catalyst which possessed single atomic Pt on the CeO_2 support and gave a full conversion of CO at 148°C with a WHSV of 200,000 mL h^{-1} $g_{cat.}^{-1}$. To our delight, H-Co_3O_4@H-C showed comparable activity to the Pt/CeO_2 catalyst that achieved complete CO transformation at 190°C at a WHSV of 210,000 mL h^{-1} $g_{cat.}^{-1}$. Taking the supervisor activity of single atom catalyst into consideration, H-Co_3O_4@H-C exhibited remarkable catalytic activity that is close to noble-metal catalysts at high WHSVs. Moreover, as shown in Fig. 7b, H-Co_3O_4@H-C also exhibited excellent durability in the oxidation of CO at 130°C with only a slight decline in activity even after 24 h of online reaction.

CONCLUSIONS

In summary, we have developed a novel structure-induced strategy to boost the quantity of oxygen vacancies of Co_3O_4 materials for efficient oxidation of CO by introducing hollow structures into the Co_3O_4 NPs.

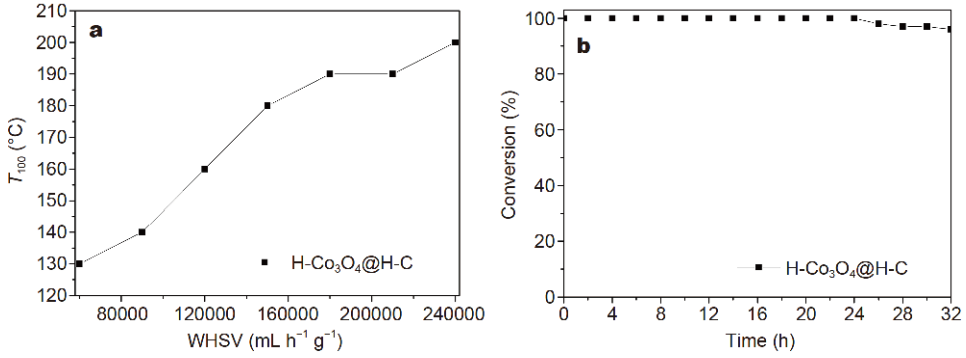

Figure 7 (a) T_{100} of H-Co_3O_4@H-C for CO oxidation at different WHSVs; (b) CO conversion as a function of reaction time for H-Co_3O_4@H-C at 130°C. All the reactions were performed under the conditions: 1 vol% CO balanced by air, $m_{cat.}$=50 mg, and WHSV=60,000 mL h^{-1} $g_{cat.}^{-1}$ except the reactions in (a) with various WHSVs.

 © Science China Press and Springer-Verlag GmbH Germany, part of Springer Nature 2019

Thus, a hollow H-Co_3O_4@H-C catalyst is successfully fabricated through reduction-oxidation with ZIF-67 as precursor. H-Co_3O_4@H-C exhibits remarkable catalytic activity, achieving a complete conversion at 130°C, which is even comparable to that of noble-metal catalysts at high WHSVs. The high activity of H-Co_3O_4@H-C would originate from the hollow Co_3O_4 NPs featured rich oxygen vacancies that could produce more O_{ads} to accelerate the CO oxidation cycle. Besides, the hollow carbon shell in H-Co_3O_4@H-C can exactly expose its inner surface which would increase the quantity of O_{ads}. The combination of the two kinds of hollow cavities enables the catalyst to retain its high catalytic activity even at very high WHSVs, and shows great durability during the longtime online reaction. The structure-induced strategy might open up a new avenue to the development of novel porous materials with richened oxygen vacancies for highly efficient and durable oxidation reactions.

Received 25 July 2019; accepted 4 September 2019; published online 22 October 2019

1 Royer S, Duprez D. Catalytic oxidation of carbon monoxide over transition metal oxides. ChemCatChem, 2011, 3: 24–65
2 Xie X, Shen W. Morphology control of cobalt oxide nanocrystals for promoting their catalytic performance. Nanoscale, 2009, 1: 50–60
3 Liotta LF, Wu H, Pantaleo G, *et al.* Co_3O_4 nanocrystals and Co_3O_4-MO_x binary oxides for CO, CH_4 and VOC oxidation at low temperatures: a review. Catal Sci Technol, 2013, 3: 3085–3102
4 Wang X, Tian W, Zhai T, *et al.* Cobalt(II,III) oxide hollow structures: fabrication, properties and applications. J Mater Chem, 2012, 22: 23310–23326
5 Sun Y, Lei F, Gao S, *et al.* Atomically thin tin dioxide sheets for efficient catalytic oxidation of carbon monoxide. Angew Chem Int Ed, 2013, 52: 10569–10572
6 Lykaki M, Pachatouridou E, Carabineiro SAC, *et al.* Ceria nanoparticles shape effects on the structural defects and surface chemistry: implications in CO oxidation by Cu/CeO_2 catalysts. Appl Catal B-Environ, 2018, 230: 18–28
7 Liu B, Li W, Song W, *et al.* Carbonate-mediated Mars-van Krevelen mechanism for CO oxidation on cobalt-doped ceria catalysts: facet-dependence and coordination-dependence. Phys Chem Chem Phys, 2018, 20: 16045–16059
8 Wang H, Feng E, Liu Y, *et al.* High-performance hierarchical ultrathin sheet-based CoOOH hollow nanospheres with rich oxygen vacancies for the oxygen evolution reaction. J Mater Chem A, 2019, 7: 7777–7783
9 Kouotou PM, Vieker H, Tian ZY, *et al.* Structure-activity relation of spinel-type Co-Fe oxides for low-temperature CO oxidation. Catal Sci Technol, 2014, 4: 3359–3367
10 Yang J, Zhou H, Wang L, *et al.* Cobalt-doped K-OMS-2 nanofibers: a novel and efficient water-tolerant catalyst for the oxidation of carbon monoxide. ChemCatChem, 2017, 9: 1163–1167
11 Yu Y, Takei T, Ohashi H, *et al.* Pretreatments of Co_3O_4 at moderate temperature for CO oxidation at −80°C. J Catal, 2009, 267: 121–128
12 Xie X, Li Y, Liu ZQ, *et al.* Low-temperature oxidation of CO catalysed by Co_3O_4 nanorods. Nature, 2009, 458: 746–749
13 Koo B, Xiong H, Slater MD, *et al.* Hollow iron oxide nanoparticles for application in lithium ion batteries. Nano Lett, 2012, 12: 2429–2435
14 Yan F, Guo D, Zhang S, *et al.* An ultra-small $NiFe_2O_4$ hollow particle/graphene hybrid: fabrication and electromagnetic wave absorption property. Nanoscale, 2018, 10: 2697–2703
15 Tianou H, Wang W, Yang X, *et al.* Inflating hollow nanocrystals through a repeated Kirkendall cavitation process. Nat Commun, 2017, 8: 1261–1269
16 Xia W, Qu C, Liang Z, *et al.* High-performance energy storage and conversion materials derived from a single metal-organic framework/graphene aerogel composite. Nano Lett, 2017, 17: 2788–2795
17 Huang K, Sun Y, Zhang Y, *et al.* Hollow-structured metal oxides as oxygen-related catalysts. Adv Mater, 2019, 31: 1801430
18 Lou XWD, Archer LA, Yang Z. Hollow micro-/nanostructures: synthesis and applications. Adv Mater, 2008, 20: 3987–4019
19 Dang S, Zhu QL, Xu Q. Nanomaterials derived from metal-organic frameworks. Nat Rev Mater, 2018, 3: 17075–17088
20 Zhao SN, Song XZ, Song SY, *et al.* Highly efficient heterogeneous catalytic materials derived from metal-organic framework supports/precursors. Coord Chem Rev, 2017, 337: 80–96
21 Shen K, Chen X, Chen J, *et al.* Development of MOF-derived carbon-based nanomaterials for efficient catalysis. ACS Catal, 2016, 6: 5887–5903
22 Zhou L, Zhuang Z, Zhao H, *et al.* Intricate hollow structures: controlled synthesis and applications in energy storage and conversion. Adv Mater, 2017, 29: 1602914–1602942
23 Yu L, Hu H, Wu HB, *et al.* Complex hollow nanostructures: synthesis and energy-related applications. Adv Mater, 2017, 29: 1604563–1604601
24 Zhao Y, Jiang L. Hollow micro/nanomaterials with multilevel interior structures. Adv Mater, 2009, 21: 3621–3638
25 Qi Z, Pei Y, Goh TW, *et al.* Conversion of confined metal@ZIF-8 structures to intermetallic nanoparticles supported on nitrogen-doped carbon for electrocatalysis. Nano Res, 2018, 11: 3469–3479
26 Zhang Y, Pan A, Ding L, *et al.* Nitrogen-doped yolk-shell-structured CoSe/C dodecahedra for high-performance sodium ion batteries. ACS Appl Mater Interfaces, 2017, 9: 3624–3633
27 Zhang Y, Pan A, Wang Y, *et al.* Self-templated synthesis of N-doped $CoSe_2$/C double-shelled dodecahedra for high-performance supercapacitors. Energy Storage Mater, 2017, 8: 28–34
28 Guo H, Li T, Chen W, *et al.* General design of hollow porous $CoFe_2O_4$ nanocubes from metal-organic frameworks with extraordinary lithium storage. Nanoscale, 2014, 6: 15168–15174
29 Salunkhe RR, Tang J, Kamachi Y, *et al.* Asymmetric supercapacitors using 3D nanoporous carbon and cobalt oxide electrodes synthesized from a single metal-organic framework. ACS Nano, 2015, 9: 6288–6296
30 Guo W, Sun W, Lv LP, *et al.* Microwave-assisted morphology evolution of Fe-based metal-organic frameworks and their derived Fe_2O_3 nanostructures for Li-ion storage. ACS Nano, 2017, 11: 4198–4205
31 Pei Y, Qi Z, Li X, *et al.* Morphology inherence from hollow MOFs to hollow carbon polyhedrons in preparing carbon-based electrocatalysts. J Mater Chem A, 2017, 5: 6186–6192
32 Shao J, Wan Z, Liu H, *et al.* Metal organic frameworks-derived Co_3O_4 hollow dodecahedrons with controllable interiors as out-

 © Science China Press and Springer-Verlag GmbH Germany, part of Springer Nature 2019

standing anodes for Li storage. J Mater Chem A, 2014, 2: 12194–12200
33 Yang Y, Wang F, Yang Q, *et al.* Hollow metal-organic framework nanospheres *via* emulsion-based interfacial synthesis and their application in size-selective catalysis. ACS Appl Mater Interfaces, 2014, 6: 18163–18171
34 Deng Y, Dong Y, Wang G, *et al.* Well-defined ZIF-derived Fe-N codoped carbon nanoframes as efficient oxygen reduction catalysts. ACS Appl Mater Interfaces, 2017, 9: 9699–9709
35 Tang J, Salunkhe RR, Liu J, *et al.* Thermal conversion of core-shell metal-organic frameworks: a new method for selectively functionalized nanoporous hybrid carbon. J Am Chem Soc, 2015, 137: 1572–1580
36 Xia BY, Yan Y, Li N, *et al.* A metal-organic framework-derived bifunctional oxygen electrocatalyst. Nat Energy, 2016, 1: 15006–15013
37 Wang W, Dahl M, Yin Y. Hollow nanocrystals through the nanoscale Kirkendall effect. Chem Mater, 2013, 25: 1179–1189
38 Yin Y, Rioux RM, Erdonmez CK, *et al.* Formation of hollow nanocrystals through the nanoscale Kirkendall effect. Science, 2004, 304: 711–714
39 Fan HJ, Gösele U, Zacharias M. Formation of nanotubes and hollow nanoparticles based on Kirkendall and diffusion processes: a review. Small, 2007, 3: 1660–1671
40 Yang Z, Yang N, Pileni MP. Nano Kirkendall effect related to nanocrystallinity of metal nanocrystals: influence of the outward and inward atomic diffusion on the final nanoparticle structure. J Phys Chem C, 2015, 119: 22249–22260
41 Yan N, Chen Q, Wang F, *et al.* High catalytic activity for CO oxidation of Co_3O_4 nanoparticles in SiO_2 nanocapsules. J Mater Chem A, 2013, 1: 637–643
42 Wu Z, Deng J, Liu Y, *et al.* Three-dimensionally ordered mesoporous Co_3O_4-supported Au–Pd alloy nanoparticles: high-performance catalysts for methane combustion. J Catal, 2015, 332: 13–24
43 Song W, Poyraz AS, Meng Y, *et al.* Mesoporous Co_3O_4 with controlled porosity: inverse micelle synthesis and high-performance catalytic CO oxidation at −60°C. Chem Mater, 2014, 26: 4629–4639
44 Wang HL, Yeh H, Chen YC, *et al.* Thermal stability of metal-organic frameworks and encapsulation of CuO nanocrystals for highly active catalysis. ACS Appl Mater Interfaces, 2018, 10: 9332–9341
45 Nie L, Mei D, Xiong H, *et al.* Activation of surface lattice oxygen in single-atom Pt/CeO_2 for low-temperature CO oxidation. Science, 2017, 358: 1419–1423

Acknowledgements This work was supported by the National Natural Science Foundation of China (21825802, 21576095 and 21436005), the Fundamental Research Funds for the Central Universities (2019PY11), the Science and Technology Program of Guangzhou (201804020009), the State Key Laboratory of Pulp and Paper Engineering (2017ZD04 and 2018TS03), and the Natural Science Foundation of Guangdong Province (2016A050502004 and 2017A030312005).

Author contributions Li Y conceived the idea and designed the experiments; Chen Z synthesized the samples and performed most of the experiments; Wang Y, Liang Q, Chen L, and Zhan W participated in some characterization and/or reaction experiments and analyze the data; Chen Z and Li Y co-wrote the paper. All authors contributed to the general discussion.

Conflict of interest The authors declare that they have no conflict of interest.

Supplementary information Supporting data are available in the online version of the paper.

Zhijie Chen received his BSc degree from South China University of Technology. He is currently a Master candidate with Prof. Yingwei Li at the School of Chemistry and Chemical Engineering, South China University of Technology, China. His current research focuses on the catalytic transformation of CO based on MOF-derived materials.

Yingwei Li received his BSc degree in 1998 and his PhD in 2003, both from Tsinghua University, and he then conducted postdoctoral work at the University of Calgary and the University of Michigan (Ann Arbor) from 2003 to 2007. He is currently a full professor at the School of Chemistry and Chemical Engineering, South China University of Technology. His research focuses on the design and synthesis of new MOF-based materials for heterogeneous catalysis.

结构诱导富集氧空位的空心Co_3O_4催化CO高效氧化

陈芝杰, 王亚晶, 梁倩楠, 陈立宇, 詹伟腾, 李映伟*

摘要 四氧化三钴(Co_3O_4)被认为是一种具有应用前景的CO氧化催化剂. 根据Mars-van Krevelen机理, Co_3O_4的氧空位对提高催化活性起到非常重要的作用. 本文提出一种新颖的结构诱导策略以制备具有丰富氧空位的空心Co_3O_4, 实现高效CO氧化. 通过还原-氧化热解过程, 金属有机骨架前驱体(如ZIF-67)被转化成镶嵌有空心Co_3O_4颗粒的空心碳壳材料. 空心Co_3O_4颗粒具有丰富的氧空位, 在130°C时能催化CO完全氧化转化, 远低于实心Co_3O_4材料的完全转化温度(220°C). 此外, 空心碳壳结构可以降低氧化过程中的分子扩散阻力. 得益于其独特的中空结构, H-Co_3O_4@H-C在高达240,000 mL h^{-1} $g_{cat.}^{-1}$的空速下显示出与贵金属催化剂相媲美的活性. 此外, H-Co_3O_4@H-C催化剂也显示出良好的稳定性, 反应24 h后活性才略微下降.

 © Science China Press and Springer-Verlag GmbH Germany, part of Springer Nature 2019